tvst

Article

Derivation and Characterization of Murine and Amphibian Müller Glia Cell Lines

Ryan A. Gallo[1,2], Farhan Qureshi[2], Thomas A. Strong[1], Steven H. Lang[1], Kevin A. Pino[1], Galina Dvoriantchikova[1], and Daniel Pelaez[1,3]

[1] Dr. Nasser Ibrahim Al-Rashid Orbital Vision Research Center, Bascom Palmer Eye Institute, Department of Ophthalmology, University of Miami Miller School of Medicine, Miami, FL, USA
[2] Medical Scientist Training Program, University of Miami Miller School of Medicine, Miami, FL, USA
[3] Department of Cell Biology, University of Miami Miller School of Medicine, Miami, FL, USA

Correspondence: Daniel Pelaez, Dr. Nasser Ibrahim Al-Rashid Orbital Vision Research Center, Department of Ophthalmology, Bascom Palmer Eye Institute, University of Miami Miller School of Medicine, 1638 NW 10th Ave, Rm 804, Miami, FL 33136, USA. e-mail: dpelaez@med.miami.edu

Received: September 24, 2021
Accepted: March 13, 2022
Published: April 4, 2022

Keywords: Müller glia; *Xenopus laevis*; cell line; purinergic signaling; P2X7

Citation: Gallo RA, Qureshi F, Strong TA, Lang SH, Pino KA, Dvoriantchikova G, Pelaez D. Derivation and characterization of murine and amphibian Müller glia cell lines. Transl Vis Sci Technol. 2022;11(4):4, https://doi.org/10.1167/tvst.11.4.4

Purpose: Müller glia (MG) in the retina of *Xenopus laevis* (African clawed frog) reprogram to a transiently amplifying retinal progenitor state after an injury. These progenitors then give rise to new retinal neurons. In contrast, mammalian MG have a restricted neurogenic capacity and undergo reactive gliosis after injury. This study sought to establish MG cell lines from the regeneration-competent frog and the regeneration-deficient mouse.

Methods: MG were isolated from postnatal day 5 GLAST-CreERT; $Rb^{fl/fl}$ mice and from adult (3–5 years post-metamorphic) *X laevis*. Serial adherent subculture resulted in spontaneously immortalized cells and the establishment of two MG cell lines: murine retinal glia 17 (RG17) and *Xenopus* glia 69 (XG69). They were characterized for MG gene and protein expression by qPCR, immunostaining, and Western blot. Purinergic signaling was assessed with calcium imaging. Pharmacological perturbations with 2′-3′-O-(4-benzoylbenzoyl) adenosine 5′-triphosphate (BzATP) and KN-62 were performed on RG17 cells.

Results: RG17 and XG69 cells express several MG markers and retain purinergic signaling. Pharmacological perturbations of intracellular calcium responses with BzATP and KN-62 suggest that the ionotropic purinergic receptor P2X7 is present and functional in RG17 cells. Stimulation of XG69 cells with adenosine triphosphate–induced calcium responses in a dose-dependent manner.

Conclusions: We report the characterization of RG17 and XG69, two novel MG cell lines from species with significantly disparate retinal regenerative capabilities.

Translational Relevance: RG17 and XG69 cell line models will aid comparative studies between species endowed with varied regenerative capacity and will facilitate the development of new cell-based strategies for treating retinal degenerative diseases.

Introduction

Müller glia (MG) are the major glial cells of the vertebrate retina. They are the only glial phenotype to originate from the retinal neuroepithelium and the last to terminally differentiate from late multipotent retinal progenitor cells.[1,2] MG perform critical supportive functions, including maintaining homeostasis, preventing neuronal excitotoxicity, removing toxic metabolic byproducts, recycling photopigments, and contributing to the blood-retina barrier, among others.[3]

Although MG development and function are highly conserved across vertebrates, their regenerative competency varies greatly from species to species.[4] In some species, MG reprogram to a transiently amplifying progenitor state after an injury, which can then give rise to new functional retinal neurons. The MG of fish and frogs display a robust injury-induced proliferative and regenerative response throughout adulthood; those of postnatal chicks proliferate after injury, but have

limited neurogenic competence; and those of MG of mice and humans fail to elicit any regeneration of the injured retina.[5–12] Instead, upon injury, mammalian MG undergo reactive gliosis, which impedes tissue repair and exacerbates neuronal degeneration.[13]

Yet, various studies indicate that mammalian MG have a dormant neurogenic capacity. When mouse MG are genetically or pharmacologically forced to reprogram, limited retinal regeneration can occur.[14–17] These findings suggest that additional factors are necessary to elicit a full regenerative response in vivo. Comparative studies between species endowed with varied regenerative properties are integral to elucidate the mechanisms that can promote MG-mediated regeneration in mammals for the treatment of retinal degenerative diseases.

In contrast with zebrafish MG, *Xenopus laevis* (African clawed frog) and mammalian MG are quiescent under normal physiologic conditions.[5–7] Yet, in the frog, retinal injury reactivates MG to regenerate the damaged retina.[10,11] Here, we report the establishment and characterization of two spontaneously immortalized MG cell lines from mice and *X laevis* frogs. These lines represent valuable resources to help us further understand organism-specific MG biology, pathophysiology, epigenetic landscape, and permissiveness for progenitor state reprogramming.

Methods

Animals

Animals were treated in accordance with the National Research Council's Guide for the Care and Use of Laboratory Animals and the ARVO Statement for the Use of Animals in Ophthalmic and Vision Research. Animal procedures were approved by the Institutional Animal Care and Use Committee at the University of Miami. We crossed GLAST-CreERT (The Jackson Laboratory, Bar Harbor, ME; stock number 012586) and $Rb^{fl/fl}$ (The Jackson Laboratory, stock number 026563) mice to generate GLAST-CreERT; $Rb^{fl/fl}$ mice. Mice were maintained in a regulated environment and fed ad libitum. Frogs were housed in a temperature-, conductivity-, and pH-controlled environment.

Cell Culture

A litter of postnatal day 5 transgenic GLAST-CreERT; $Rb^{fl/fl}$ mice pups were euthanized, and their globes were enucleated. Retinas were dissected free of the retinal pigment epithelium (RPE), lens, cornea, and iris. Retinas were dissociated by incubation in phosphate-buffered saline (PBS) containing 16.5 U/mL activated papain (Worthington, Lakewood, NJ) and 124 U/mL DNase (Sigma-Aldrich, St. Louis, MO) for 30 minutes at 37°C with gentle trituration. Digestion was stopped with ovomucoid (Worthington), and retinal cells were pelleted by centrifugation (300 g, 5 minutes) and resuspended in high-glucose Dulbecco's modified Eagle Medium (ThermoFisher Scientific, Waltham, MA) containing 10% fetal bovine serum (Denville Scientific, Hollistion, MA), 1% sodium pyruvate, and 1% antibiotic–antimycotic. The cells were passed through a 40 µM cell strainer before plating. Cells were maintained at 37°C in humidified 5% CO_2, and the medium was changed every 3 days. We used 0.25% trypsin-EDTA (ThermoFisher Scientific) for the dissociation of adherent cells. Adherent MG became enriched after 2 to 3 passages as identified by cell morphology.

Globes were collected from euthanized wild-type adult (3–5 years postmetamorphic) *X laevis*, and the retinas were dissected and then dissociated by incubation in 0.25% trypsin-EDTA at room temperature for 1 hour while shaking at 1000 rpm. Trypsinization was inactivated with Leibovitz's L-15 Medium (ThermoFisher Scientific) supplemented with 28% sterile deionized water, 10% fetal bovine serum (Denville Scientific), and 1% antibiotic–antimycotic. Retinal cells were pelleted by centrifugation (300 g, 5 minutes), resuspended in complete Leibovitz's L-15 medium, and then passed through a 40-µM cell strainer before plating. Cells were maintained at 20°C to 23°C in a humidified chamber with media changes every 3 days. After 3 to 4 weeks, frog retinal cell colonies became prominent after initial plating. Adherent MG became enriched after 2 to 3 passages as identified by cell morphology. We used 0.25% trypsin-EDTA (ThermoFisher Scientific) for the dissociation of adherent cells with a 7-minute incubation at room temperature. To culture the frog RPE, choroid/sclera from multiple globes were dissected free from the retina and incubated in 0.25% trypsin-EDTA at room temperature for 1 hour while shaking at 1000 rpm. Trypsinization was inactivated with complete medium, and the cells were passed through a 40-µM cell strainer before culturing. RPE enrichment was confirmed based on morphology, pigmentation, and PAX6 immunostaining.

Polymerase Chain Reaction (PCR) Analysis

To determine Cre-mediated recombination, purified DNA from RG17 cells was subjected to PCR amplification using the primers listed in Table 1.[18] DNA

Table 1. PCR Primers

Primer	Sequence	Notes
Rb212	GAAAGGAAAGTCAGGGACATTGGG	To determine *Rb1* recombination[18]
Rb18	GGCGTGTGCCATCAATG	
Rb19E	CTCAAGAGCTCAGACTCATGG	
10110	ACAATCTGGCCTGCTACCAAAGC	To identify GLAST-CreERT transgene (The Jackson Laboratory)
10112	CCAGTGAAACAGCATTGCTGTC	

Table 2. Antibodies Used for Immunofluorescence Staining and Western Blot

Antibodies	Source and Cat#	Host	Dilution	RRID
Beta Actin	ThermoFisher Scientific Cat# MA5-15739	Mouse	1:2000^{WB}	AB_10979409
CRALBP	ThermoFisher Scientific Cat# MA1-813	Mouse	1:1000^{WB}	AB_2178528
GFAP	Abcam Cat# ab10062	Mouse	1:1000^{IF}	AB_296804
GLAST (EAAT1)	Abcam Cat# ab416	Rabbit	1:200^{IF} 1:1000^{WB}	AB_304334
GS	Millipore Cat# MAB302	Mouse	1:200^{IF} 1:1000^{WB}	AB_2110656
Pax6	BioLegend Cat# 901301	Rabbit	1:100^{IF}	AB_2565003
RPE65	ThermoFisher Scientific Cat# MA1-16578	Mouse	1:1000^{WB}	AB_2181003
Sox9	ThermoFisher Scientific Cat# PA5-81966	Rabbit	1:200^{IF} 1:1000^{WB}	AB_2789127
Vimentin	Abcam Cat# ab7783	Rabbit	1:100^{IF} 1000^{WB}	AB_2833071
ZO-1	ThermoFisher Scientific Cat# 61-7300	Rabbit	1:1000^{WB}	AB_2533938
Alexa Fluor 488	Abcam Cat# ab150113	Goat	1:100^{IF}	AB_2576208
Alexa Fluor 594	Abcam Cat# ab150112	Donkey	1:1000^{IF}	AB_2813898
Alexa Fluor 647	Abcam Cat# ab150079	Goat	1:1000^{IF}	AB_2722623
Mouse IgG HRP-conjugated antibody	R&D Systems Cat# HAF007	Goat	1:1000^{WB}	AB_357234
Rabbit IgG HRP-conjugated antibody	R&D Systems Cat# HAF008	Goat	1:1000^{WB}	AB_357235

samples were extracted with the DNeasy Blood & Tissue Kit (Qiagen, Hilden, Germany). The PCR program included 35 cycles of 30 seconds at 94°C, 30 seconds at 58°C, and 50 seconds at 72°C. Primers 10110 and 10112 were used for GLAST–CreERT transgene identification as provided by the Jackson Laboratory.

Short Tandem Repeat (STR) Analysis

STR DNA analysis on RG17 cells (passages 5 and 20) was performed by the ATCC Mouse Cell Line STR Profiling Service (Manassas, VA).

Immunofluorescence Staining

Cells were fixed in 4% paraformaldehyde in PBS for 15 minutes at room temperature. Adult frog and mice globes were fixed in 4% paraformaldehyde in PBS for 2 hours, then placed in a 15% to 30% sucrose/PBS gradient. Globes were embedded in Tissue-Tek O.C.T. Compound (Torrance, CA) for frozen sectioning (12 µm). The cells and tissue specimens were blocked with PBS containing 10% normal donkey serum and 0.2% Triton X-100 for 2 hours. Primary antibodies (listed in Table 2) in blocking solution were applied overnight at 4°C. AlexaFlour (Abcam, Cambridge, MA) secondary antibodies were applied for 1 hour at room temperature. We used 4', 6-diamidino-2-phenylindole (1 µg/mL; Bio-Rad Laboratories, Hercules, CA; #1351303) to counterstain. Specificity of labeling was confirmed by omitting the primary antibody. Imaging was performed on a Leica AOBS SP8 confocal microscope (Leica Microsystems, Exton, PA).

Table 3. qPCR Primers

Gene	Forward	Reverse
	Mouse	
GS	GGGGACAAATGCGGAGGTTA	AAAGTCTTCGCACACCCGAT
GLAST	CTGGTAACCCGGAAGAACCC	GGGGAGCACAAATCTGGTGA
Rlbp1	CGTGGAAGGCAGAGTTAAAGGC	CAAGGATCACATCCAAGATGGG
Sox9	TCCCCGCAACAGATCTCCTA	GAGCCGGAGTTCTGATGGTC
Vim	AGCAGTATGAAAGCGTGGCT	CTCCAGGGACTCGTTAGTGC
β actin	GATCAGCAAGCAGGAGTACGA	AAAACGCAGCTCAGTAACAGTC
	Frog	
GS.L	ACAAACTTGCTGAGGAAACGAAG	CGAAGTTCCATTCAGGGATTTCATC
GLAST.L	GCCGTAGACTGGTTTTTGGAC	TGAGCTCGTGCCTAGACAAA
Sox9.L	CTGGGGAAGTTATGGAGGCTTT	CAGCCTGTAGGGCCTTGAAA
Vim.L	ACAATCTGGCCGATGATCTCC	GGCATTGTCCACATCCTGTCT
ef1α.S[46]	TGGATATGCCCCTGTGTTGGATT	TCCACGCACATTGGCTTTCCT

Quantitative PCR (qPCR)

Total RNA from mouse and frog MG (passage 4–6 [primary] and passage 20–25 cells) were extracted using the RNeasy Plus Kit (Qiagen) then reverse transcribed with Superscript III polymerase (Invitrogen, Carlsbad, CA). A qPCR was performed with a QuantStudio 7 Flex Real-Time PCR System (Applied Biosystems, Waltham, MA) using PowerUp SYBR Green Master Mix (Applied Biosystems). Primers are listed in Table 3. Relative expression was calculated using 2ˆdelta delta Ct with *β-actin* and *efl1α.s* as the housekeeping genes for mouse and frog samples, respectively. Three independent cultures of both primary and late passaged cells were run in triplicate. Data are presented as the geometric mean ± geometric standard deviation of the three independent cultures. The unpaired *t*-test was applied with a *P* value of 0.05 or less considered statistically significant.

Western Blot

Cells were lysed with radioimmunoprecipitation assay buffer (ThermoFisher Scientific) containing protease and phosphatase inhibitors. Cell lysates were resuspended in 2× Laemmli buffer (Bio-Rad Laboratories) with 5% β-mercaptoethanol and equal amounts of total protein were loaded into precast SDS-PAGE gels (Bio-Rad Laboratories). After transfer to polyvinylidene difluoride membranes (Bio-Rad Laboratories), these membranes were blocked with 5% bovine serum albumin in Tris-buffered saline containing 0.1% Tween 20. Lysates were probed with the antibodies listed in Table 2. Blots were incubated with horseradish peroxidase-conjugated species-specific secondary antibodies (R&D Systems, Minneapolis, MN). Proteins were visualized with an enhanced chemiluminescence substrate (Bio-Rad Laboratories).

Growth Curve

Growth curves were generated with the CellTiter-Glo Luminescent Cell Viability Assay (Promega, Madison, WI) as described previously.[19] We plated 1000 cells per well of a 96-well plate with complete medium, and luminescence was measured with a SpectraMax MiniMax 300 Imaging Cytometer (Molecular Devices, San Jose, CA). Growth curves were generated for primary MG and passage 20 cells for both the mouse and frog. Media was changed daily. Triplicate cultures for each group were plated in each assay. Values graphed represent the mean ± standard deviation of the luminescent signal from each culture. An exponential growth model (GraphPad Prism 6 v9.0.2; San Diego, CA) was applied to estimate doubling times.

Calcium Imaging and Quantification

RG17 and XG69 cells were plated on glass cover slips and incubated in the calcium indicator Fluo-4, acetoxymethyl ester in complete media for 30 minutes. The media were then aspirated, and cells were immersed in physiological buffer (125 mmol/L NaCl, 5.9 mmol/L KCl, 2.56 mmol/L $CaCl_2$, 1 mmol/L $MgCl_2$, 25 mmol/L HEPES, and 0.1% bovine serum albumin, pH 7.4) for imaging on a Leica TCS SP5 upright confocal microscope (Leica Microsystems). Adenosine triphosphate (ATP) disodium (50 µM;

Selleck Chemicals, Houston, TX, Cat# S1985), KN-62 (1 μM; Selleck Chemicals, Cat# S7422), 2′-3′-O-(4-benzoylbenzoyl) adenosine 5′-triphosphate (50 μM; BzATP) triethylammonium salt (Tocris, Minneapolis, MN, Cat# 3312), and glutamate (100–1000 μM) were used. Cytosolic calcium levels were quantified as described by Makhmutova et al.[20] Changes in fluorescence intensity were expressed as percentage changes over baseline (ΔF/F). Baseline was defined as the mean of the intensity values during the nonstimulatory period. Data are displayed as heat maps to include all recorded cells from two to three independent cultures. To measure the overall integrated calcium response, the area under the curve for each response was calculated with GraphPad Prism 6 v9.0.2 (San Diego, CA).

Results

Establishment and Characterization of a Mouse MG Cell Line

Primary retinal cells were cultured from postnatal day 5 transgenic GLAST-CreERT; $Rb^{fl/fl}$ mice pups. After two to three passages, a homogenous MG population was isolated and identified by cell morphology. Serial adherent subculture of the isolated MG resulted in spontaneously immortalized cells and the establishment of the retinal glia 17 (RG17) line. Of note, these cells have not been induced to undergo Cre-mediated recombination (Supplementary Fig. S1).

RG17 cells have been maintained for more than 40 passages, grow as an adherent monolayer, and present an invariant morphology. Phenotypic expression of well-characterized mammalian MG markers was observed through 20 passages. Immunofluorescence staining shows RG17 cells express glutamine synthetase (GS), glutamate–aspartate transporter (GLAST; also known as excitatory amino acid transporter 1 [EAAT1]), Sox9, and vimentin (Fig. 1A). RG17 cells stained a characteristic punctate pattern for GLAST throughout the cytoplasm. RG17 cells do not stain for glial fibrillary acidic protein (GFAP), which is not an MG-specific marker, but rather an index of gliosis. The specificity of the antibodies was confirmed with staining on mouse retinas (Supplementary Fig. S2).

A qPCR was performed to compare gene expression levels of MG characteristic genes between primary MG and RG17 cells (passages 20–25). There were no significant changes in *Glast*, *Sox9*, and *Vim* expression. *GS* expression decreased 36.7% ($P = 0.0023$) and *Rlbp1* expression decreased 94.9% ($P = 0.002$) in RG17 compared with the primary MG (Fig. 1B). Protein expression of GS, GLAST, Sox9, vimentin, and cellular retinaldehyde binding protein (CRALBP, encoded by *Rlbp1*) at passage 20 was confirmed by Western blot. CRALBP protein expression greatly decreased with cell culture passaging, which is consistent with the qPCR results (Fig. 1C).

Under standard culture conditions, passage 5 RG17 cells have a doubling time of 58.47 hours (95% confidence interval [CI], 54.04–63.39) and passage 20 RG17 cells have a doubling time of 60.90 hours (95% CI, 57.18–64.96) (Fig. 1D). No changes in the morphologic presentation or the growth rate were observed after cryopreservation and recovery. The STR profiles of passage 5 and passage 20 RG17 cells are consistent, indicating that the cell line is stable with respect to the analyzed loci over the time frame of these passages (Supplementary Fig. S3).

Establishment and Characterization of a *X laevis* MG Cell Line

Primary retinal cells and RPE were isolated and cultured from the retinas of adult wild-type (3–5 years postmetamorphic) *X laevis* frogs. Cell colonies formed after approximately 3 weeks in culture, and multiple morphologically distinct populations were present. One major cell population was made up of large adherent cells with prominent nuclei, epithelial-like morphology, and broad processes, similar to cultured mammalian MG. A second major population was identified as RPE cells based on their phenotypic characteristics on phase contrast microscopy. This population consisted of flat, adherent, pigmented cells with an epithelial-like morphology and expressed the RPE marker PAX6 on immunofluorescence staining (Supplementary Fig. S4). RPE cells were not observed in culture after the third passage. The remaining adherent cell population was expanded and achieved homogeneous cell morphology. These cells expressed GS on immunofluorescence staining, a known marker of MG in *X laevis*, through 25 passages.[21] These spontaneously immortalized MG cells were named *Xenopus* glia 69 (XG69).

Along with GS, XG69 cells also express the classical mammalian MG markers GLAST, Sox9, and vimentin on immunofluorescence staining through 20 passages (Fig. 2A). They were negative for GFAP, consistent with the fact that *X laevis* lack the GFAP gene.[22] The specificity of these antibodies was confirmed with staining on adult *X laevis* retinas. Sox9 staining was not MG specific in the adult frog retina, but had strong nuclear staining in the cultured MG (Supplementary Fig. 2). qPCR showed that there were no significant

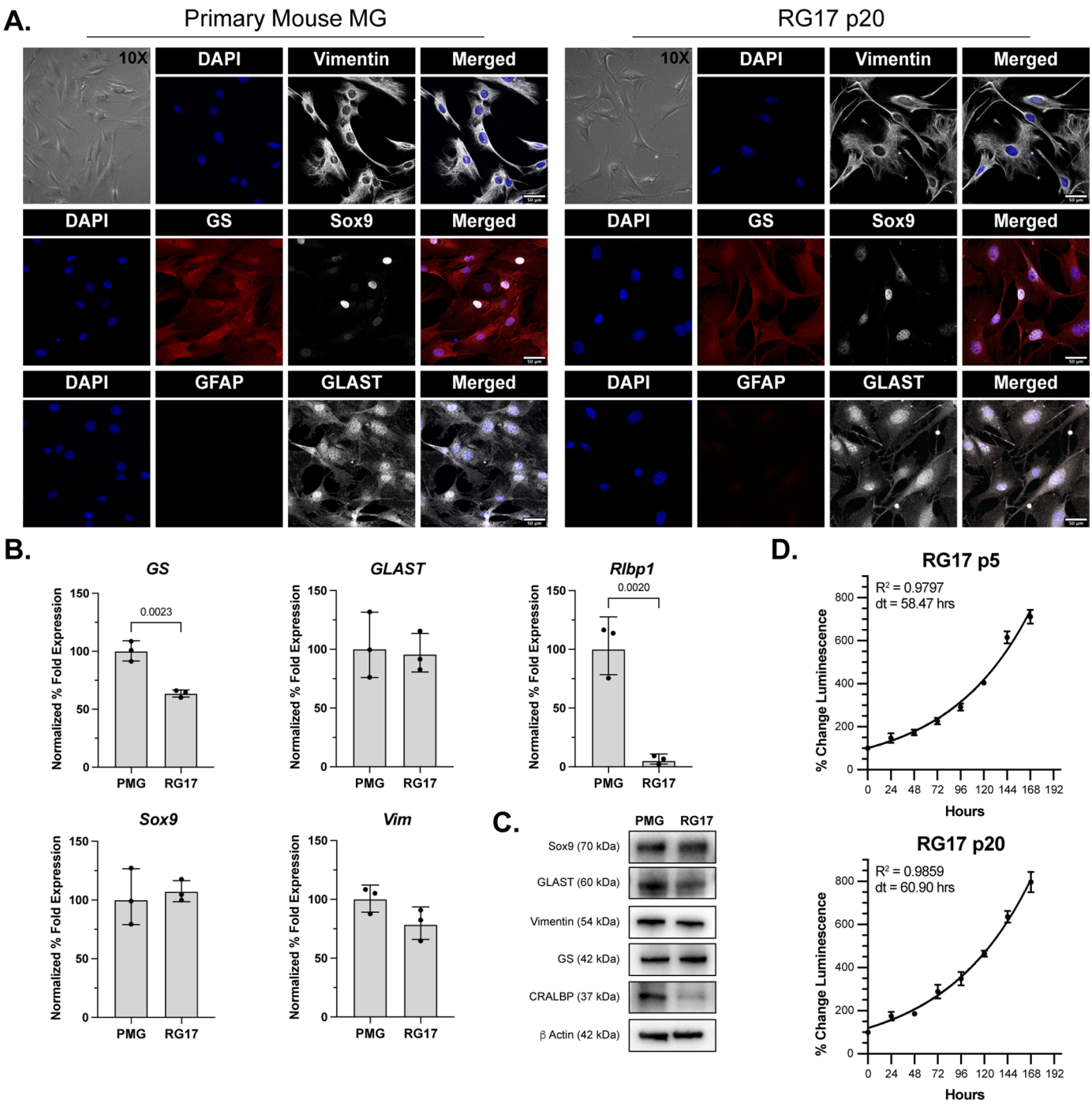

Figure 1. Immunophenotypic characterization of mouse MG cell line RG17. (A) Phase contrast images and immunofluorescence staining of primary MG cells and passage 20 RG17 cells. RG17 demonstrate typical MG morphology in culture and express many well-characterized MG markers. Scale bar, 50 µm and applies to all immunofluorescence images. (B) Expression of characteristic MG genes in primary MG and RG17 cells (passages 20–25). The geometric means and geometric standard deviations ($N = 3$ independent cultures) are graphed. An unpaired *t*-test was applied with a *P* value of ≤ 0.05 considered statistically significant. (C) Western blot detection of MG markers from primary MG and passage 20 RG17 cells. (D) The doubling rate of RG17 cells does not vary significantly between passages 5 and 20. Data points are mean $\pm$ standard deviation.

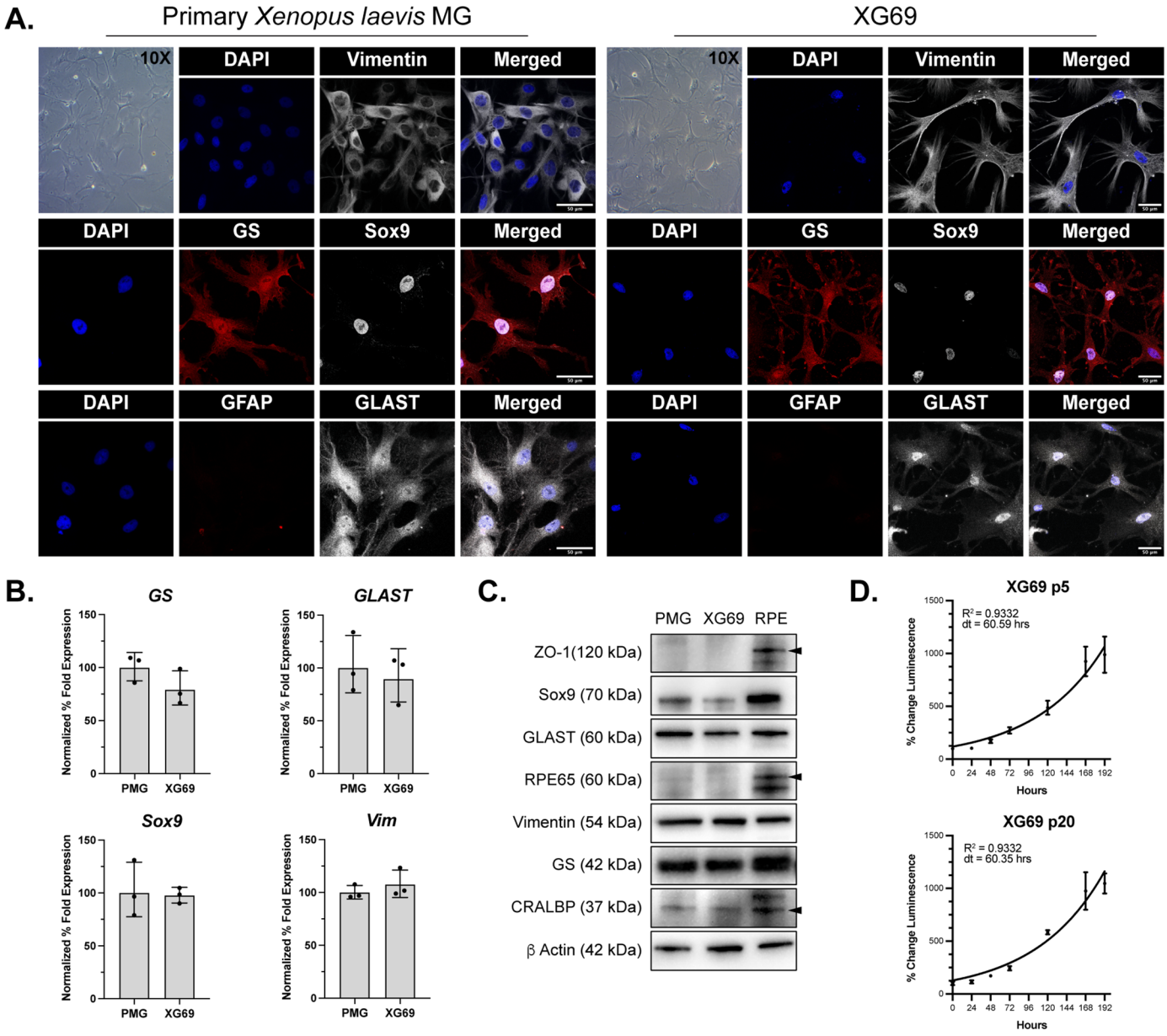

Figure 2. Immunophenotypic characterization of *X laevis* MG cell line XG69. (A) Phase contrast images and immunofluorescence staining of primary MG and XG69 cell line at passage 20. (B) Expression of MG genes in primary MG and XG69 cells (passages 20–25). The geometric means and geometric standard deviations ($N = 3$ independent cultures) are graphed. An unpaired *t*-test was applied with a *P* value of ≤ 0.05 considered statistically significant. (C) Western blot detection of MG markers from primary MG and passage 20 XG69 cells. Frog MG do not express RPE markers ZO-1 and RPE65 unlike primary *Xenopus* RPE cells. (D) The doubling rate of XG69 cells does not vary significantly through 20 passages. Data points are mean ± standard deviation.

differences in expression of *GS*, *Vim*, *GLAST*, and *Sox9* between primary MG and passage 20 XG69 (Fig. 2B). Western blot confirmed protein expression of GLAST, GS, Sox9, vimentin, and CRALBP. Frog MG did not express ZO-1 and RPE65 on Western blot, unlike primary frog RPE cells (Fig. 2C).

After serial adherent subculture, XG69 maintain a constant morphology and growth rate. Passage 5 XG69 cells have a doubling time of 60.59 hours (95% CI, 51.15–71.95) and passage 20 XG69 cells have a doubling time of 60.35 hours (95% CI, 50.51–72.55) (Fig. 2D). They do not show any changes in growth rate or morphology after cryopreservation and recovery.

P2X7 Purinergic Signaling in RG17

In the presence of 50 µM ATP, RG17 cells exhibited large calcium responses with an average peak

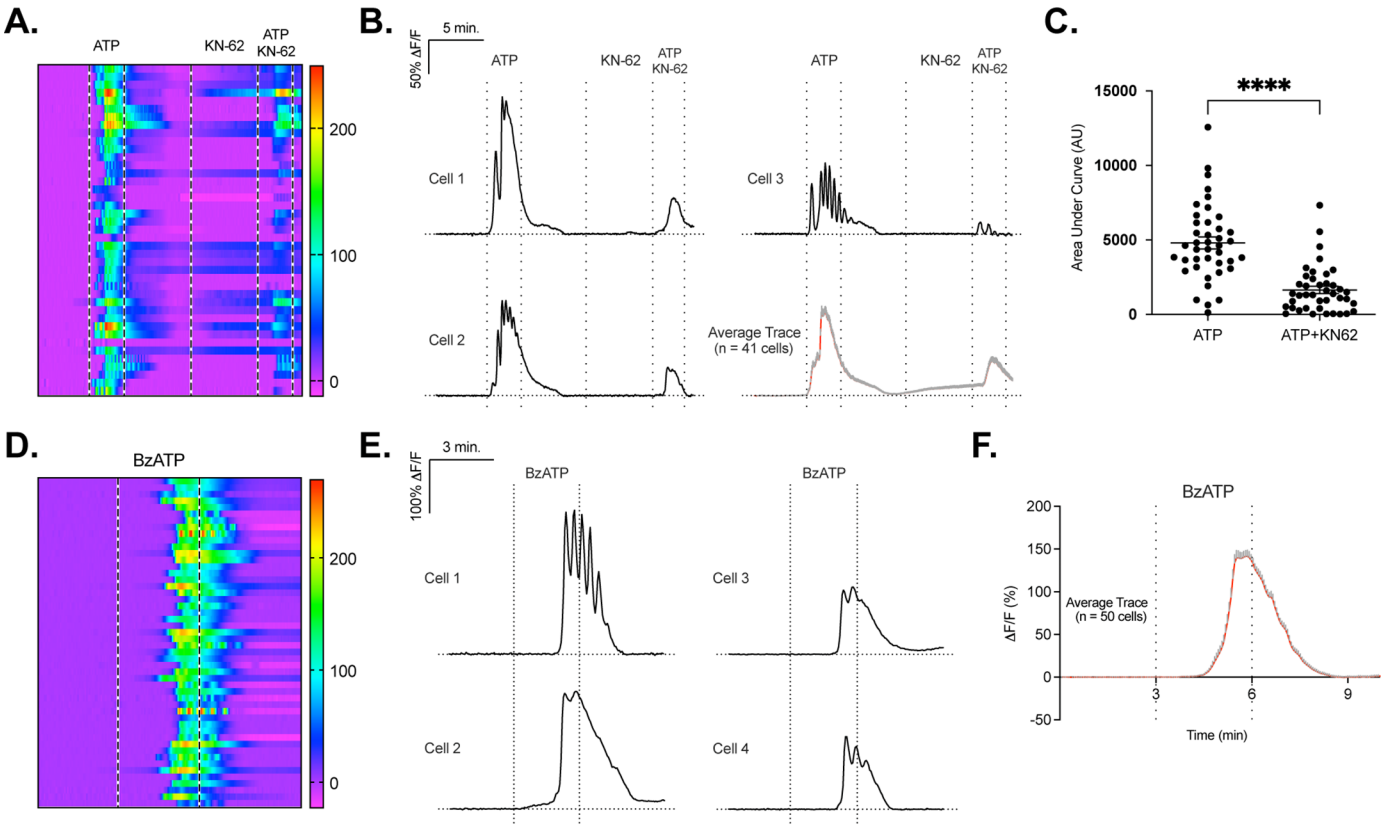

Figure 3. Calcium responses elicited by P2X7 activation in RG17 cells. (A) Heat map shows calcium responses of RG17 cells to 50 µM of ATP and the combination of 50 µM of ATP and 1 µM of P2X7 noncompetitive antagonist P2X7 ($n = 41$ cells). Each row is a single cell, the x axis is time, and the change of the fluorescent intensity over baseline (ΔF/F) is indicated by the color scale, where fluorescence intensity increases from purple to red. (B) Confocal images of the RG17 intracellular calcium responses. Scale bar, 100 µm. (C) Representative traces of calcium responses of individual RG17 cells as well as the average trace to ATP and KN-62. (D) KN-62 mitigated the ATP-induced calcium response in RG17 cells (unpaired t-test of the area under the curve; **** $P < 0.0001$). (E) Heat map shows calcium responses of RG17 cells to 50 µM of BzATP ($n = 50$ cells). Each row is a single cell, the x axis is time, and ΔF/F is indicated by the color scale, where fluorescence intensity increases from purple to red. (F) Representative traces of calcium responses of individual RG17 cells to BzATP. (G) Average trace of the RG17 calcium response to BzATP ($n = 50$ cells).

percentage change of fluorescent intensity over baseline (ΔF/F) of 91.39 ± 7.11%. 82% (50/61) of RG17 cells exhibited calcium responses with kinetic variations after ATP stimulation (Supplementary Fig. S5, Supplementary Movie 1).

To examine the mechanisms underlying the ATP-evoked responses, we pharmacologically perturbed calcium signaling with the P2X7 receptor noncompetitive antagonist KN-62 (Figs. 3A–B, Supplementary Movie 2). The average peak ΔF/F of RG17 cells was 123.27 ± 8.06% with ATP alone, whereas it was 50.65 ± 6.66% with both ATP and 1 µM KN-62 (Fig. 3B). KN-62 significantly decreased the ATP-evoked calcium response according to an area under the curve analysis ($P < 0.0001$) (Fig. 3C). In contrast, the application of 50 µM of P2X7 agonist BzATP elicited robust intracellular calcium responses, with an average peak ΔF/F of 141.47 ± 7.34% (Figs. 3D–F, Supplementary Movie 3). Together, these observations provide pharmacological evidence for the presence of functional P2X7 receptors in RG17 cells.

Purinergic Signaling of XG69

XG69 cells exhibited a lower uptake of the Fluo-4, AM calcium indicator compared with RG17 cells. Nonetheless, intracellular calcium responses were observed after XG69 cells were treated with increasing concentrations of ATP (Fig. 4A, Supplementary Movie 4). Small spontaneous calcium transients were also detected from many cells before ATP stimulation. Variations in calcium response kinetics were observed (Fig. 4B). In the presence of 50 µM ATP, the average peak ΔF/F was 4.58 ± 1.13%. The average peaks were 2.84 ± 0.75% and 6.044 ± 1.11% with 100 µM and 300 µM ATP stimulation, respectively (Fig. 4C).

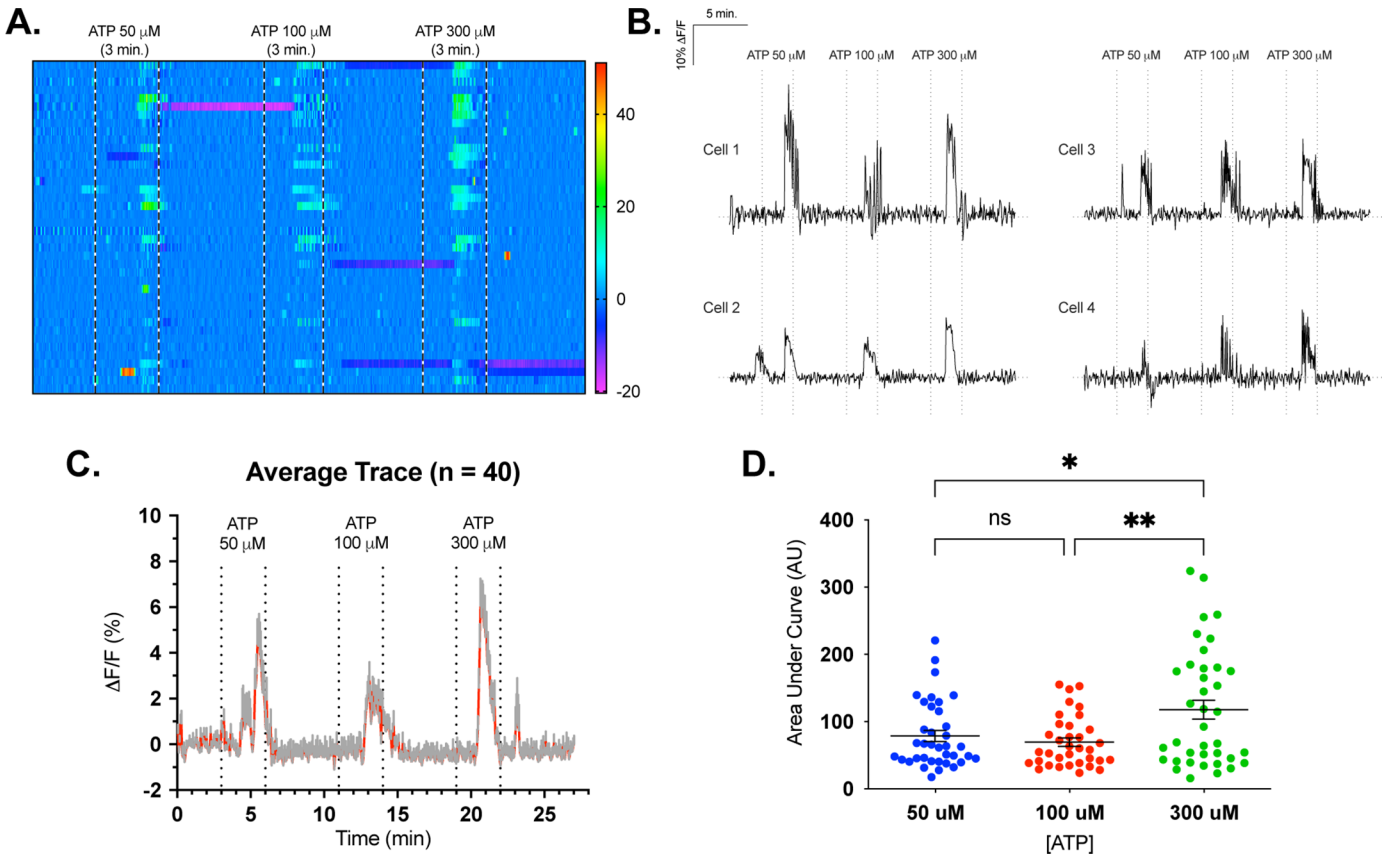

Figure 4. ATP elicits calcium responses in XG69 cells. (A) Heat map of calcium responses from all recorded XG69 cells to 50, 100, and 300 μM of ATP ($n = 40$ cells). Each row is a single cell, the x axis is time, and ΔF/F is indicated by the color scale, where fluorescence intensity increases from purple to red. (B) Representative calcium response traces from individual XG69 cells. (C) Average trace of calcium responses ($n = 40$ cells). (D) XG69 cells exhibit intracellular calcium increases with a dose–response to ATP stimulation (ordinary one-way analysis of variance of the area under the curve, $^*P < 0.05$, $^{**}P < 0.01$).

XG69 cells treated with increasing ATP concentrations induced calcium responses in a statistically significant dose-dependent manner according to an area under the curve analysis (Fig. 4D). The investigation of P2X7 signaling in XG69 was unsuccessful; the pharmacological agents and/or prolonged incubation times affected cell viability. Last, glutamate (100, 300, and 1000 μM) did not evoke intracellular calcium increases in XG69 cells, confirming that these cells did not arise from retinal neurons (Supplementary Fig. S6).

Discussion

We report the derivation and characterization of two spontaneously immortalized MG cell lines from organisms with significantly disparate retinal regenerative competencies: the murine RG17 cell line and the amphibian XG69 cell line. The establishment of these resources will facilitate comparative studies of MG regenerative mechanisms.

MG can reprogram to a transiently amplifying progenitor state to regenerate neurons upon retinal injury or degeneration. However, this neurogenic competence varies greatly among vertebrates.[4] In the uninjured fish retina, MG continuously give rise to rod photoreceptors, acting as a reservoir of rod precursors.[5,6] Upon injury, fish MG revert to a multipotent progenitor state that regenerates the damaged retina.[8,9] Although *X laevis* were long known to have extensive eye regenerative abilities, only recently were their MG reported to proliferate and be the source of de novo retinal neurogenesis.[10,11] Frog MG are reactivated in an age-dependent manner, with older animals displaying more efficient proliferation.[11] In the postnatal chick, MG proliferate after injury, but possess limited regenerative competence.[12] Conversely, mouse and human MG fail to elicit any functional regeneration of the injured retina and instead undergo reactive gliosis.[13]

Nevertheless, mammalian MG have a dormant regenerative capacity. They have significant transcriptomic and epigenomic overlap with late retinal progenitor cells and have low levels of methylation in genes associated with pluripotency, which suggests that they are primed to dedifferentiate.[23–26] Studies of fish MG-mediated retinal regeneration have inspired strategies for stimulating retinal regeneration in mammals. However, when adult mammalian MG are genetically forced to reprogram, extremely limited regeneration of only certain retinal neuronal phenotypes occurs.[14–16] These findings suggest that a full regenerative response, including the establishment of amplifying progenitors, requires additional molecular components. Cross-species transcriptomic and epigenomic analyses of MG from species with varied regenerative competence have identified different signaling pathways, transcription factors, and gene regulatory networks influencing the MG injury response.[27] Further functional validation of these identified elements is necessary. Our cell lines can aid in the investigation of transcriptional and epigenetic factors, as well as extrinsic factors, that modulate proliferation and neurogenic competence in MG.

Several mammalian MG cell lines derived from mice, rats, or humans have been generated by both spontaneous immortalization and forced expression of viral oncogenes. Each cell line has its own unique characteristics and can be used to study different aspects of MG biology. The spontaneously immortalized human MIO-M1 and conditionally immortalized mouse ImM10 cell lines exhibit progenitor characteristics.[28–31] The spontaneously immortalized QMMuC-1 cell line was established from postnatal day 7 C57BL/6J mice and has similar electrophysiological characteristics and glycolytic capacity as primary MG.[32] Isolated from light-damaged Sprague-Dawley rat retinas, the rMC-1 cells are simian virus 40 immortalized and strongly express GFAP, a marker of reactive gliosis.[33] TR-MUL5 cells are a conditionally immortalized rat MG cell line.[34] A spontaneously immortalized rat MG cell line, named SIRMu-1, was reported to have a more similar transcriptome to primary MG than rMC-1 cells.[35]

Unlike other mouse MG cell lines, the RG17 line originates from a litter of postnatal day 5 transgenic GLAST-CreERT; $Rb^{fl/fl}$ mice. Thus, the line contains a tamoxifen-inducible *Cre* recombinase driven by the MG-specific GLAST promoter element and a homozygous Rb1-floxed allele ($Rb^{fl/fl}$) genotype. Cell cycle reentry and proliferation are essential to harnessing the full potential of MG-mediated endogenous regeneration. Although various signaling pathways and growth factors have been identified to stimulate MG proliferation in fish and chicks, mammalian MG proliferation is limited. After retinal injury, mouse MG downregulate the cyclin kinase inhibitor $p27^{Kip1}$ and re-enter G1 phase of the cell cycle, but seldom divide owing to cyclin D3 regulation.[36] Because Cip/Kip family cyclin kinase inhibitors regulate cell cycle progression by blocking phosphorylation of the tumor suppressor *RB1*, we generated GLAST-CreERT; $Rb^{fl/fl}$ mice to explore how direct inactivation of *RB1* in MG affects their proliferation.[37]

While working with MG isolated from GLAST-CreERT; $Rb^{fl/fl}$ mice pups, one culture was maintained for more than 40 passages without tamoxifen-induced *Cre* activity. The mechanism of spontaneous immortalization remains to be determined. RG17 cells express many well-characterized MG markers, including GS, Sox9, Vimentin, GLAST, and CRALBP (Figs. 1A–C). Although retinal astrocytes may also express vimentin and GS, they do not express CRALBP. When comparing primary MG with passage 20 RG17 cells, most MG marker transcripts and proteins were expressed at similar levels. CRALBP transcript and protein expression decreased with passaging compared with primary MG. This is also observed in the rat SIRMu-1 cell line.[35] CRALBP in MG in vivo is involved in photopigment recycling and helps to maintain cone photoreceptor function.[38,39] Along with the culture conditions, the absence of cone photoreceptors and chemical cues may lead to the CRALBP downregulation observed in the RG17 line. The transcript levels of *GS* also decreased in RG17 cells with passaging, likely owing to culture conditions that have insufficient regulators of MG *GS* expression, such as secreted factors from RPE or glucocorticoid hormones.[40]

In addition, we performed functional purinergic signaling characterization on RG17 cells with calcium imaging. Purinergic signaling has important roles in bidirectional neuron–glia signaling, homeostatic MG functions, and contributes to reactive gliosis under pathological conditions.[41] MG express various metabotropic P2Y purinergic receptor subtypes, and human MG have also been reported to express the ionotropic P2X7 receptor.[42,43] P2X7 signaling has been suggested to contribute to proliferative gliosis.[44] When RG17 cells were stimulated with ATP, they displayed a variety of response kinetics suggesting that multiple types of purinergic receptors may be activated (Supplementary Fig. S5). We sought to determine if RG17 express functional P2X7 receptors, which has not been reported in other mouse MG cell lines. The ATP-induced calcium response was significantly diminished with P2X7 receptor noncompetitive antagonist KN-62 (Figs. 3A–C), whereas the P2X7 agonist BzATP evoked large intracellular calcium responses (Figs. 3D–F). Together, these data provide pharmaco-

logical proof of functional P2X7 receptors in RG17 cells.

To the best of our knowledge, the establishment and characterization of a nonmammalian MG cell line has not been reported. The XG69 cell line is the first MG cell line generated from the retina of the nonmammalian vertebrate *X laevis*. The mechanism of spontaneous immortalization is unknown. These cells originate from adult frogs whose MG exhibit robust proliferative responses upon injury.[11] They express an array of MG markers and do not express RPE-specific protein markers ZO-1 or RPE65 (Figs. 2A–C). CRALBP expression was low in both primary and later passaged cells, which is likely due culture conditions, as described previously. The XG69 cells retain purinergic signaling capacity, and we show a dose-dependent response to ATP (Fig. 4). It was not possible to deduce the mechanisms underlying the purinergic response because the small molecules and the prolonged incubation time in the recording buffer affected cell viability. Intracellular calcium increases were also absent after glutamate application, which suggests that they were not derived from retinal neurons.[45] Together, these findings confirm that XG69 cells originate from primary *X laevis* MG and retain functional purinergic signaling.

In summary, we describe the establishment and characterization of the murine RG17 cell line and the frog XG69 cell line. The MG of frogs have a remarkable ability to regenerate the damaged retina and restore visual function, whereas mammalian MG fail to elicit any regeneration of the injured retina. These cell lines will facilitate a better understanding of MG biology, pathophysiology, and regenerative competence across these species. Studies on XG69 cells may help validate regulators of MG reprogramming and inspire new strategies to stimulate mammalian MG-mediated retinal regeneration.

Acknowledgments

The authors thank Dawn A. Owens and Michelle G. Zhang for their assistance with the *X laevis*.

Supported in part by the Dr. Nasser Al-Rashid Orbital Research Fund (Miami, FL, USA). The Bascom Palmer Eye Institute is supported by NIH Center Core Grant P30EY014801 and a Research to Prevent Blindness Unrestricted Grant (New York, NY, USA). RG and FQ were supported in part by NIH MSTP T32 GM112601. RG was supported in part by a Research Fellowship from the VitreoRetinal Surgery Foundation (Edina, MN, USA).

Disclosure: **R.A. Gallo,** None; **F. Qureshi,** None; **T.A. Strong,** None; **S.H. Lang,** None; **K.A. Pino,** None; **G. Dvoriantchikova,** None; **D. Pelaez,** None

References

1. Young RW. Cell-differentiation in the retina of the mouse. *Anat Rec*. 1985;212(2):199–205.
2. Turner DL, Cepko CL. A common progenitor for neurons and glia persists in rat retina late in development. *Nature*. 1987;328(6126):131–136.
3. Bringmann A, Pannicke T, Grosche J, Francke M, Wiedemann P, Skatchkov SN, et al. Muller cells in the healthy and diseased retina. *Prog Retin Eye Res*. 2006;25(4):397–424.
4. Levi T, Reh TA. Comparative biology of vertebrate retinal regeneration: restoration of vision through cellular reprogramming. *Cold Spring Harb Perspect Biol*. 2021 Sep 27;a040816.
5. Raymond PA, Barthel LK, Bernardos RL, Perkowski JJ. Molecular characterization of retinal stem cells and their niches in adult zebrafish. *BMC Dev Biol*. 2006;6:36.
6. Bernardos RL, Barthel LK, Meyers JR, Raymond PA. Late-stage neuronal progenitors in the retina are radial Muller glia that function as retinal stem cells. *J Neurosci*. 2007;27(26):7028–7040.
7. Hamon A, Roger JE, Yang XJ, Perron M. Muller glial cell-dependent regeneration of the neural retina: An overview across vertebrate model systems. *Dev Dyn*. 2016;245(7):727–738.
8. Powell C, Cornblath E, Elsaeidi F, Wan J, Goldman D. Zebrafish Muller glia-derived progenitors are multipotent, exhibit proliferative biases and regenerate excess neurons. *Sci Rep*. 2016;6:24851.
9. Lenkowski JR, Raymond PA. Muller glia: stem cells for generation and regeneration of retinal neurons in teleost fish. *Prog Retin Eye Res*. 2014;40:94–123.
10. Hamon A, Garcia-Garcia D, Ail D, Bitard J, Chesneau A, Dalkara D, et al. Linking YAP to Muller glia quiescence exit in the degenerative retina. *Cell Rep*. 2019;27(6):1712–1725.e6.
11. Langhe R, Chesneau A, Colozza G, Hidalgo M, Ail D, Locker M, et al. Muller glial cell reactivation in Xenopus models of retinal degeneration. *Glia*. 2017;65(8):1333–1349.
12. Fischer AJ, Reh TA. Muller glia are a potential source of neural regeneration in the postnatal chicken retina. *Nat Neurosci*. 2001;4(3):247–252.
13. Bringmann A, Wiedemann P. Muller glial cells in retinal disease. *Ophthalmologica*. 2012;227(1):1–19.

14. Jorstad NL, Wilken MS, Grimes WN, Wohl SG, VandenBosch LS, Yoshimatsu T, et al. Stimulation of functional neuronal regeneration from Muller glia in adult mice. *Nature*. 2017;548(7665):103–107.
15. Yao K, Qiu S, Wang YV, Park SJH, Mohns EJ, Mehta B, et al. Restoration of vision after de novo genesis of rod photoreceptors in mammalian retinas. *Nature*. 2018;560(7719):484–488.
16. Ueki Y, Wilken MS, Cox KE, Chipman L, Jorstad N, Sternhagen K, et al. Transgenic expression of the proneural transcription factor Ascl1 in Muller glia stimulates retinal regeneration in young mice. *Proc Natl Acad Sci USA*. 2015;112(44):13717–13722.
17. Todd L, Hooper MJ, Haugan AK, Finkbeiner C, Jorstad N, Radulovich N, et al. Efficient stimulation of retinal regeneration from Muller glia in adult mice using combinations of proneural bHLH transcription factors. *Cell Rep*. 2021;37(3):109857.
18. Marino S, Vooijs M, van Der Gulden H, Jonkers J, Berns A. Induction of medulloblastomas in p53-null mutant mice by somatic inactivation of Rb in the external granular layer cells of the cerebellum. *Genes Dev*. 2000;14(8):994–1004.
19. Gallo RA, Lang SH, Gomez A, Sabater AL, Tse DT, Pelaez D, et al. Effects of mitomycin-C and 5-fluorouracil on ocular adnexal sebaceous carcinoma cells. *Am J Ophthalmol*. 2022 Jan 4;S0002-9394(21)00660-7.
20. Makhmutova M, Weitz J, Tamayo A, Pereira E, Boulina M, Almaca J, et al. Pancreatic beta-cells communicate with vagal sensory neurons. *Gastroenterology*. 2021;160(3):875–888.e11.
21. Jablonski MM, Iannaccone A. Targeted disruption of Muller cell metabolism induces photoreceptor dysmorphogenesis. *Glia*. 2000;32(2):192–204.
22. Martinez-De Luna RI, Ku RY, Aruck AM, Santiago F, Viczian AS, San Mauro D, et al. Muller glia reactivity follows retinal injury despite the absence of the glial fibrillary acidic protein gene in Xenopus. *Dev Biol*. 2017;426(2):219–35.
23. Blackshaw S, Harpavat S, Trimarchi J, Cai L, Huang H, Kuo WP, et al. Genomic analysis of mouse retinal development. *PLoS Biol*. 2004;2(9):E247.
24. Roesch K, Jadhav AP, Trimarchi JM, Stadler MB, Roska B, Sun BB, et al. The transcriptome of retinal Muller glial cells. *J Comp Neurol*. 2008;509(2):225–238.
25. Dvoriantchikova G, Seemungal RJ, Ivanov D. Development and epigenetic plasticity of murine Muller glia. *Biochim Biophys Acta Mol Cell Res*. 2019;1866(10):1584–1594.
26. Powell C, Grant AR, Cornblath E, Goldman D. Analysis of DNA methylation reveals a partial reprogramming of the Muller glia genome during retina regeneration. *Proc Natl Acad Sci USA*. 2013;110(49):19814–19819.
27. Hoang T, Wang J, Boyd P, Wang F, Santiago C, Jiang L, et al. Gene regulatory networks controlling vertebrate retinal regeneration. *Science*. 2020;370(6519):eabb8598.
28. Limb GA, Salt TE, Munro PM, Moss SE, Khaw PT. In vitro characterization of a spontaneously immortalized human Muller cell line (MIO-M1). *Invest Ophthalmol Vis Sci*. 2002;43(3):864–869.
29. Lawrence JM, Singhal S, Bhatia B, Keegan DJ, Reh TA, Luthert PJ, et al. MIO-M1 cells and similar muller glial cell lines derived from adult human retina exhibit neural stem cell characteristics. *Stem Cells*. 2007;25(8):2033–2043.
30. Otteson DC, Phillips MJ. A conditional immortalized mouse muller glial cell line expressing glial and retinal stem cell genes. *Invest Ophthalmol Vis Sci*. 2010;51(11):5991–6000.
31. Phillips MJ, Otteson DC. Differential expression of neuronal genes in Muller glia in two- and three-dimensional cultures. *Invest Ophthalmol Vis Sci*. 2011;52(3):1439–1449.
32. Augustine J, Pavlou S, O'Hare M, Harkin K, Stitt A, Curtis T, et al. Characterization of a spontaneously immortalized murine Muller glial cell line QMMuC-1. *Invest Ophthalmol Vis Sci*. 2018;59(3):1666–1674.
33. Sarthy VP, Brodjian SJ, Dutt K, Kennedy BN, French RP, Crabb JW. Establishment and characterization of a retinal Muller cell line. *Invest Ophthalmol Vis Sci*. 1998;39(1):212–216.
34. Tomi M, Funaki T, Abukawa H, Katayama K, Kondo T, Ohtsuki S, et al. Expression and regulation of L-cystine transporter, system xc-, in the newly developed rat retinal Muller cell line (TR-MUL). *Glia*. 2003;43(3):208–217.
35. Kittipassorn T, Haydinger CD, Wood JPM, Mammone T, Casson RJ, Peet DJ. Characterization of the novel spontaneously immortalized rat Muller cell line SIRMu-1. *Exp Eye Res*. 2019;181:127–135.
36. Dyer MA, Cepko CL. Control of Muller glial cell proliferation and activation following retinal injury. *Nat Neurosci*. 2000;3(9):873–880.
37. Hengst L, Reed SI. Inhibitors of the Cip/Kip family. *Curr Top Microbiol Immunol*. 1998;227:25–41.
38. Das SR, Bhardwaj N, Kjeldbye H, Gouras P. Muller cells of chicken retina synthesize 11-cis-retinol. *Biochem J*. 1992;285(Pt 3):907–913.

39. Xue Y, Shen SQ, Jui J, Rupp AC, Byrne LC, Hattar S, et al. CRALBP supports the mammalian retinal visual cycle and cone vision. *J Clin Invest*. 2015;125(2):727–738.
40. Germer A, Jahnke C, Mack A, Enzmann V, Reichenbach A. Modification of glutamine synthetase expression by mammalian Muller (glial) cells in retinal organ cultures. *Neuroreport*. 1997;8(14):3067–3072.
41. Wurm A, Pannicke T, Iandiev I, Francke M, Hollborn M, Wiedemann P, et al. Purinergic signaling involved in Muller cell function in the mammalian retina. *Prog Retin Eye Res*. 2011;30(5):324–342.
42. Fries JE, Goczalik IM, Wheeler-Schilling TH, Kohler K, Guenther E, Wolf S, et al. Identification of P2Y receptor subtypes in human muller glial cells by physiology, single cell RT-PCR, and immunohistochemistry. *Invest Ophthalmol Vis Sci*. 2005;46(8):3000–3007.
43. Pannicke T, Fischer W, Biedermann B, Schadlich H, Grosche J, Faude F, et al. P2X7 receptors in Muller glial cells from the human retina. *J Neurosci*. 2000;20(16):5965–5972.
44. Bringmann A, Pannicke T, Moll V, Milenkovic I, Faude F, Enzmann V, et al. Upregulation of P2X(7) receptor currents in Muller glial cells during proliferative vitreoretinopathy. *Invest Ophthalmol Vis Sci*. 2001;42(3):860–867.
45. Uckermann O, Vargova L, Ulbricht E, Klaus C, Weick M, Rillich K, et al. Glutamate-evoked alterations of glial and neuronal cell morphology in the guinea pig retina. *J Neurosci*. 2004;24(45):10149–10158.
46. Fini JB, Le Mevel S, Palmier K, Darras VM, Punzon I, Richardson SJ, et al. Thyroid hormone signaling in the Xenopus laevis embryo is functional and susceptible to endocrine disruption. *Endocrinology*. 2012;153(10):5068–5081.

Supplementary Material

Supplementary Movie 1. ATP induces intracellular calcium responses in RG17 cells. Scale bar, 100 µm.

Supplementary Movie 2. Pharmacological effects of P2X7 antagonist KN-62 on ATP-induced intracellular calcium responses in RG17 cells. Scale bar, 100 µm.

Supplementary Movie 3. Intracellular calcium responses induced by P2X7 agonist BzATP in RG17 cells. Scale bar, 100 µm.

Supplementary Movie 4. ATP dose-response activation of intracellular calcium responses in XG69 cells. Scale bar, 100 µm.